Journal of Colloid and Interface Science 384 (2012) 10–21

Contents lists available at SciVerse ScienceDirect

Journal of Colloid and Interface Science

www.elsevier.com/locate/jcis

Preparation of controlled gold nanoparticle aggregates using a dendronization strategy

Julieta I. Paez [a], Eduardo A. Coronado [b,*], Miriam C. Strumia [a,*]

[a] IMBIV-CONICET, Departamento de Química Orgánica, Facultad de Ciencias Químicas, Universidad Nacional de Córdoba, Haya de la Torre y Medina Allende, Ciudad Universitaria, X5000HUA Córdoba, Argentina
[b] INFIQC-CLCM-CONICET, Departamento de Fisicoquímica, Facultad de Ciencias Químicas, Universidad Nacional de Córdoba, Haya de la Torre y Medina Allende, Ciudad Universitaria, X5000HUA Córdoba, Argentina

ARTICLE INFO

Article history:
Received 13 February 2012
Accepted 18 June 2012
Available online 26 June 2012

Keywords:
Dendronization
Gold nanoparticles
Nanoparticle aggregates
Self-assembly

ABSTRACT

In this work, a dendronization strategy was used to control interparticle spacing and the optical properties of gold nanoparticle (NP) aggregates in aqueous media. To achieve this goal, two dendritic disulfides bearing different functionalities on their periphery were synthesized and used as ligands to dendronize gold NPs. The dendronized NPs then undergo aggregation; this process was followed by UV–vis spectroscopy, dynamic light scattering (DLS), and transmission electronic microscopy (TEM) measurements and correlated with Generalized Mie Theory electrodynamics calculations. For comparison, NP functionalization was also studied using a nondendritic ligand. It was found that the use of dendritic disulfides allows for the preparation of controlled NP aggregates. This study demonstrates how different dendronization parameters, such as disulfide concentration, temperature, time and nature of the ligand (dendritic vs nondendritic), determine the control exerted over the size and stability of the NP aggregates.

1. Introduction

Traditionally, the aggregation of metallic nanoparticles (NPs) had been considered an undesirable process. Indeed, one of the fundamental aspects of research on the synthesis and morphological control of NPs had centered on colloidal stabilization, with the aim of avoiding aggregation [1]. However, researchers then visualize the aggregation of NP building blocks as a useful approach toward applications, which require tailored structures and functionalities [1]. NPs are considered excellent candidates for applications in nanotechnology, and the use of their nanoscale properties requires the ability of controlled processing and assembly [1]. In particular, NP assembly has been an important challenge because of the difficulty in manipulating interparticle properties. Both covalent and noncovalent interactions have proved to be crucial in the construction and exploitation of functional nanostructures, as well as in the manipulation of either the stability or the reversibility of the assembly/disassembly of NP aggregates [2].

NPs and NP assemblies exhibit unique electrical, optical, magnetic, and catalytic properties as derived from two factors: the dramatic increase in the surface area/volume ratio as the particle size is reduced, and the emergence of collective and nanoscale properties as a result of the interparticle arrangement or assembly [2]. The exploration of such nanostructures has drawn a growing interest in research studies in chemistry, physics, biology, and materials science [2]. It is well-known that the range of application of gold NP aggregates is vast, and the use of the interparticle coupling effect with practical purposes constitutes a common denominator [3]. In this respect, is worth mentioning their application in biodiagnostics [4,5], such as the determination of nucleic acids [6] or glucose sensing for diabetics [7]. In addition, the color associated with the NPs was found to be tunable as platforms for chemical sensing [3,5,8] using aggregation events, namely, the highly sensitive and selective detection of toxic metallic ions like Hg(II) [9]. As NPs have a high surface-to-volume ratio, NP aggregation reduces the solvent-exposed surface area, a very useful feature for applications in catalysis [10]. Moreover, the optical properties of NPs and NP aggregates have also been exploited in order to enhance the sensitivity of several spectroscopic techniques including Surface Enhanced Raman Spectroscopy (SERS), absorption, fluorescence, or Surface Plasmon Resonance (SPR) [3,11].

Dendritic molecules are highly ordered, regularly branched, monodisperse macromolecules. Due to their unique and well-defined macromolecular structure, they are attractive scaffolds for a variety of high-end applications, constituting a fascinating nanoscale toolkit, which rapidly accesses nanostructures through self-assembly fabrication methods [12,13]. An excellent example of this feature is the dendronization process, which involves the covalent or supramolecular interaction of dendrons with dendritic or

* Corresponding authors. Tel.: +54 351 4334170/73x120; fax: +54 351 4334170/73x151 (M.C. Strumia).
E-mail addresses: julieta@fcq.unc.edu.ar (J.I. Paez), coronado@fcq.unc.edu.ar (E.A. Coronado), mcs@fcq.unc.edu.ar (M.C. Strumia).

0021-9797/$ - see front matter © 2012 Elsevier Inc. All rights reserved.
http://dx.doi.org/10.1016/j.jcis.2012.06.034

nondendritic substrates to create well-defined, stable molecular level nanostructures [14]. Dendronization offers the possibility of obtaining materials with dendritic properties in an easy and rapid way, which could lead to improved levels of commercialization and their uses in new applications. Our own group has been working on the dendronization of different organic [15–17] and inorganic substrates [18–20] demonstrating that this is a valuable synthetic strategy toward the construction of hybrid materials with desired functions [21].

Dendronization has been used, for example, to synthesize, functionalize, and stabilize NPs. Particularly, the dendronization of gold NPs has led to the preparation of tailored nanomaterials in the last decade [22–34]. Smith et al. directly compared different dendritic structures for NP stabilization and indicated how the behavior of these hybrid materials can be subtly controlled by simple synthetic tuning of the dendritic architecture [35]. In another interesting approach, Zhong et al. reported the use of dendritic arenethiols as capping molecules to set the NP surface reactivity and interparticle assembly [36].

Additionally, the use of dendritic molecules as intermediates for controlled NP assembly has recently become a subject of study. Rotello et al. first proposed that the use of dendrimers as separate entities to space and regulate the interparticle distance is advantageous for being more modular and able to be carried out with synthetically accessible building blocks [37]. Therefore, this group [38,39] and others [40] have used dendrimers as spacers to control interparticle distance following the "bricks and mortar" approach so as to tailor dipolar coupling and control the optical response. However, further studies aiming at revealing the relationship between the dendritic structure used and the control exerted over the resulting NP aggregates are still needed. Although dendronization has been employed for NP synthesis and functionalization, we noticed the lack of systematic studies about using dendronization as a strategy to induce controlled NP aggregation.

Therefore, herein, we report on the use of a dendronization strategy to control interparticle spacing and the optical properties of gold NP aggregates in aqueous media. Two dendritic disulfides bearing different functionalities on their periphery were synthesized and used as ligands to dendronize gold NPs. The dendronized NPs then undergo aggregation; this process was followed by UV–vis spectroscopy, DLS and TEM measurements and correlated with Generalized Mie Theory electrodynamics calculations. The main objective of this work is evaluating how different dendronization parameters such as the disulfide concentration, temperature, and nature of the ligand determine the control exerted over the size and stability of the NP aggregates.

2. Experimental

2.1. Materials

Analytical-grade chemicals were used. 3,3′-dithiodipropionic acid (**1**, Aldrich), dendron Aminotriester NTN1963 (**2**, Frontier Scientific), N,N′-Dicyclohexylcarbodiimide (DCC, Aldrich), 1-hydroxybenzotriazole (HOBT, Aldrich), N,N-Dimethylformamide (DMF, Ciccarelli), sodium tetrachloroaurate(III) hydrate (Aldrich), sodium citrate (Aldrich), dichloromethane (DCM, Ciccarelli), sodium bicarbonate ($NaHCO_3$, Anedra), formic acid (85%, Ciccarelli), anhydrous methanol (MeOH, Ciccarelli) and ethanol (EtOH, Ciccarelli) were used as received. Water was purified with a Millipore Milli-Q system. All solutions were prepared immediately before use.

2.2. Instrumentation and measurements

^{1}H-NMR and ^{13}C-NMR were performed on a *Bruker Avance II* (400.16 MHz, BBI probe, Z-gradient) spectrometer at 25 °C using $CDCl_3$ or methanol-d_4 (Aldrich) as solvents. Chemical shifts (δ) were quoted in parts per million referenced to the solvent residual peak and coupling constants (*J*) in Hz. FT-IR measurements were carried out on a *Nicolet*-5SXC. Samples were prepared by pressing a mixture of solid compound with KBr to obtain pellets. Mass spectra were recorded on a Bruker, MicroTOF Q II equipment, fitted with an ESI source operated in both positive and negative modes, using nitrogen as a nebulizing and drying gas and sodium formiate 10 mM as an internal calibrant. UV–vis experiments were measured on a Shimadzu MultiSpect 1501 spectrometer. The spectra were recorded between 300 and 800 nm at 25 and at 35 °C. For the temporally resolved spectra, measurements were taken at 10-min intervals. DLS studies were conducted on a Nicomp Model 380 Submicron Particle Sizer at 25 °C. Each sample was measured twice, and the results were reproducible. TEM images were obtained with a JEM 1200EXII-JEOL electron microscope operating at 80 kV. Samples for TEM were prepared by drop-casting one drop of the colloid onto standard carbon-coated Formvar films copper grids (200-mesh), followed by the solvent natural evaporation. For each sample, at least four typical regions were scanned. The images were analyzed using the ImageJ software. The mean particle diameter and standard deviation were calculated by counting at least 150 particles from the enlarged photographs.

2.3. Synthesis

2.3.1. Synthesis of disulfide ligands

2.3.1.1. Synthesis of dendritic disulfide 3. A modified strategy originally proposed by Smith's group [35] was followed. In a flask equipped with magnetic stirrer, non-dendritic diacid disulfide **1** (0.300 g, 1.4 mmol, 1 eq) was placed and dissolved in DMF (6 mL). Subsequently, dendron **2** (1.4545 g, 3.5 mmol, 2.2 eq) was dissolved in DMF (2 mL) and added to the solution. Afterward, HOBT (0.4208 g, 3.11 mmol, 2.5 eq) and DCC (0.6491 g, 3.11 mmol, 2.5 eq) were dissolved in DMF (2 mL each) and added to the solution. The solution was stirred at room temperature for 48 h. The precipitated urea by-product was removed by filtration. The supernatant was dissolved in 20 mL of DCM, and washed twice with cold 1.5 N HCl solution, water, saturated $NaHCO_3$ solution, and water again. The organic phase was dried ($CaCl_2$) and concentrated in rotavapor. Purification was achieved using silica gel chromatography (DCM/MeOH, 95:5) to afford **3** as a white solid. The yield was 85%. **^{1}H NMR** (400 MHz, $CDCl_3$) δ_H = 6.21 (2H, s, NH); 2.93 (4H, pseudo-t, J_1 = 6.84, J_2 = 6.80, SCH_2); 2.51 (4H, pseudo-t, J_1 = 6.80, J_2 = 6.76, SCH_2CH_2); 2.23 (12H, dd, J_1 = 8.24 Hz, J_2 = 7.40, CH_2CO_2t-Bu); 1.97 (12H, dd, J_1 = 8.24, J_2 = 7.40, $CH_2CH_2CO_2$tBu); 1.43 (54H, s, —CH_3 *t*-Bu). **^{13}C NMR** (100 MHz, $CDCl_3$) δ_C = 172.87 (C═O ester), 170.17 (C═O amide), 80.63 (—$C(CH_3)_3$), 57.69 ($NHCR_3$), 36.31 (SCH_2CH_2), 33.91 (SCH_2), 29.95 ($CH_2CH_2CO_2$tBu), 29.81 (CH_2CO_2t-Bu), 28.07 (—CH_3 *t*-Bu). **IR** ν_{max} = 3325*m* (NH), 2978*m*, 2935*m* (CH), 1731*s* (C═O ester), 1655*m* (C═O amide), 1542*m* (CONH), 1368*m*, 1155*s* (—CO_2— ester). ***m/z*** (ESI QTOF+) $C_{50}H_{88}N_2O_{14}S_2$ $[M]^+$ requires 1004.5677. $[M + Na]^+$ requires 1027.5569; found: 1027.5625.

2.3.1.2. Synthesis of dendritic disulfide 4. In a flask equipped with a magnetic stirrer, disulfide **3** (0.120 g, 0.119 mmol) and formic acid were added until solid was completely covered (2 mL). The mixture was stirred at 55 °C for 16 h. The solvent was then distilled off under reduced pressure to obtain **4** as a white solid. Conversion: quantitative, yield: 96%. **^{1}H NMR** (400 MHz, MeOD) δ_H = 7.50 (2H, s, NH); 2.95 (4H, pseudo-t, J_1 = 7.04, J_2 = 6.84, SCH_2); 2.61 (4H, pseudo-t, J_1 = 6.84, J_2 = 7.00, SCH_2CH_2); 2.30 (12H, dd, J_1 = 10.36, J_2 = 8.60, CH_2COOH); 2.03 (12H, dd, J_1 = 10.40, J_2 = 8.52, CH_2CH_2COOH). **^{13}C NMR** (100 MHz, MeOD) δ_C = 177.14 (C═O acid), 173.28 (C═O amide), 58.81 ($NHCR_3$), 36.86 (SCH_2CH_2), 35.35

(SCH_2), 30.44 (CH_2CH_2COOH), 29.25 (CH_2COOH). **IR** ν_{max} = 3287*m* (OH acid), 3092*m* (NH amide), 2955*m*, 2924*m* (CH), 1712–1696*s* (C=O acid), 1654*s* (C=O amide), 1559*m* (CONH), 1454*m*, 1414*m*, 1370*m*, 1297*m*. ***m/z*** (ESI QTOF-) $C_{26}H_{40}N_2O_{14}S_2$ $[M-H]^-$ requires 667.1848; found: 667.1898. $[M-2H]^{2-}$ requires 333.0888; found: 333.0903.

2.3.2. NP synthesis and their functionalization using disulfides as ligands

13-nm gold NPs were synthesized in aqueous media according to the Turkevich's procedure [41]. A ruby red colloid was obtained. These NPs were then modified using disulfides as ligands. In order to make the comparisons meaningful, in all the functionalization experiments, we have defined the *N* parameter as a figure of merit. *N* represents the number of disulfide molecules added per NP in the organic modification process. This number was calculated as follows:

$$N = (V_{add} \times C_M)/(V_{NP} \times C_{NP})$$

where V_{add} is the volume of the disulfide solution added to functionalize the NPs, C_M is the concentration of the disulfide solution, V_{NP} is the volume of the colloid and C_{NP} is the concentration of the colloidal dispersion.

The NP modification using disulfides as ligands was performed as follows. Methanolic solutions of disulfides **1**, **3**, or **4** in proper concentrations (range of 78.750–0.0315 mM) were first prepared. Secondly, in a 5-mL volumetric flask, 1 mL of 1.58 nM NPs (*ca.* 9.49×10^{11} NPs) and 2 mL of water were mixed. Then, 0.5 mL of methanolic disulfide solution in appropriate concentration was added. Rapidly, the volume was completed with water until reaching 5 mL. The final composition of the solvent was 10% methanol in water. The temperature of all colloids was controlled using a thermostatic bath at 25 and 35 °C. The resulting modified NPs were characterized immediately after their preparation.

3. Computational details

3.1. Geometry optimizations of the different molecules

The calculations were performed with the GAUSSIAN 03 computational package [42]. All geometries were optimized and computed using a semi-empirical calculation AM1 [43]. The stationary points were localized with the Berny algorithm [44]. Neither frequency nor multiconformational analyses have been done. The calculations were carried out over the corresponding thiols [36] considering that thiolates are the adsorbed species. The molecular length of the corresponding thiolates (henceforth referred to as **3′**, **4′**, and **1′**, see Fig. S1) was estimated considering that, in a thiol monolayer-protected NP, all sulfur atoms bind to only one gold atom [45] and that the average S—Au distance is 2.4 Å [46,47].

3.2. Theoretical simulations of the optical response of the sphere clusters

The calculations were performed using the exact Generalized Multiparticle Mie Theory (GMM). The details of this method have been described elsewhere [48,49] (for details, see Supporting Information).

The calculations here presented correspond to clusters of noble metal nanospheres of the same diameter *D* = 13 or 15 nm, located in a cubic lattice with and edge-to-edge separation of 1.1; 1.8, and 2.3 nm containing 8, 19, 32, 81, 127, 179, and 280 gold spheres, matching the positions of the sphere centers in such a way to mimic an almost spherical shape aggregate (see Fig. S5). These interparticle distances (*i.e.*, edge-to-edge separations) were estimated according to the following approximations: (1) each disulfide molecule self-assemblies onto the NP surface through the disulfide moiety, being the adsorbed species the corresponding thiolates. Therefore, the organic layer length was assumed to be the thiolate molecular length; (2) the interparticle distance was therefore estimated to be twice the thiolate molecular length.

4. Results

4.1. Estimation of the molecular length of the thiolates

The estimated molecular lengths of the corresponding isolated thiolates were as follows: **3′** = 1.15 nm; **4′** = 0.91 nm; and **1′** = 0.54 nm (see Figs. S2–S4). These values will then be used to calculate the optical response of the aggregates.

4.2. Synthesis of new dendritic disulfides

The dendritic molecules were designed to contain a disulfide moiety as a core, which can be used to self-assemble the dendritic molecule onto the NP surface. From the synthetical point of view, working with disulfides is easier than working with the analogous

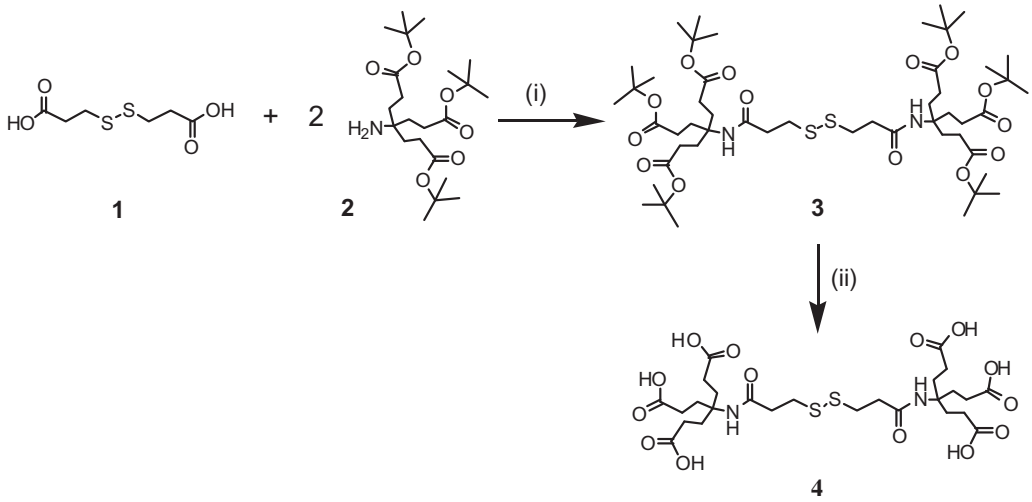

Fig. 1. Synthesis of dendritic disulfides. Reagents and reaction conditions: (i) DCC, HOBT, DMF, r.t. 48 h and (ii) HCOOH, 55 °C, overnight.

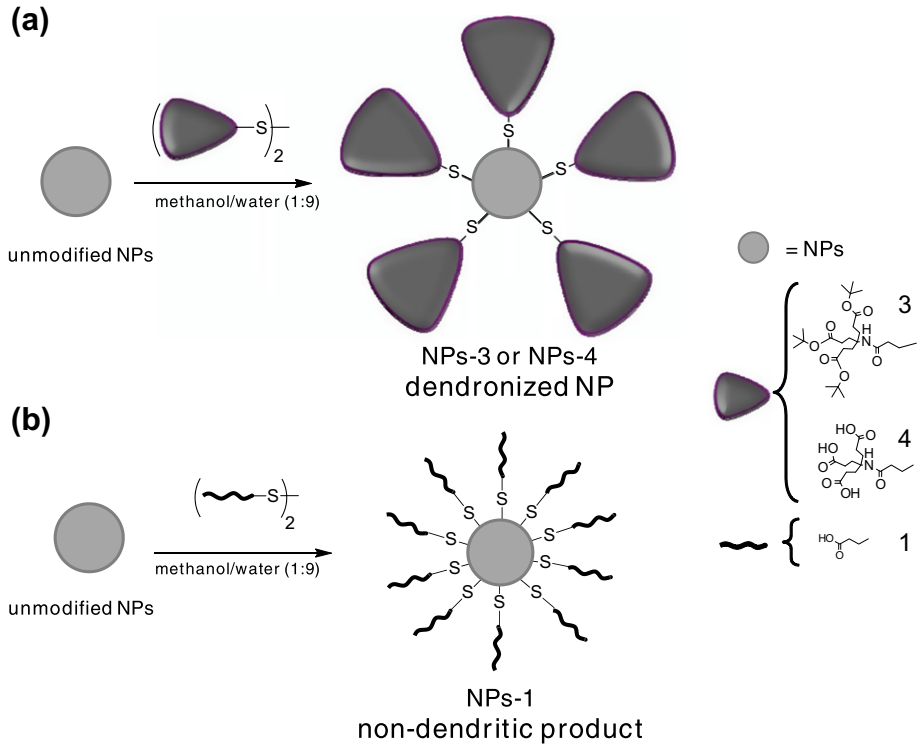

Fig. 2. Schematic representation of NP modification using (a) dendritic disulfides **3** or **4** and (b) nondendritic disulfide **1**.

thiol-functionalized structures as the latter were found to oxidize in reaction workup [50].

Fig. 1 shows the synthetic path to obtain two first-generation dendritic disulfides, **3** and **4**. Both compounds were synthesized in an easy and straightforward pathway with very good yields. Reaction (i) involves the synthesis of dendritic disulfide **3** from nondendritic disulfide **1** and Newkome-type dendron **2**. DCC and HOBT were used to activate the carboxylic acid groups of **1**. On the other hand, reaction (ii) involves the hydrolysis of the *t*Bu-ester peripheral groups of **3** to obtain compound **4**. In order to deprotect the ester groups without affecting the previously formed amide bonds, formic acid was employed.

The synthesized dendritic disulfides have different molecular size and terminal functionality: **3** shows a hydrophobic periphery given by the presence of the *t*-Bu groups, whereas **4** presents a hydrophilic surface due to its terminal carboxylic acid groups. These differences are expected to be crucial to exert control upon the resulting aggregates.

4.3. NP synthesis and their modification using the disulfides

It was considered that an important prerequisite to prepare NP aggregates with controlled optical properties was to have unmodified NPs with a narrow distribution of size and shape. In order to fulfill this condition, the Turkevich's procedure [41] was chosen to synthesize the NPs, where controllable sizes in the order of tens of nanometers can be achieved by adjustment of the gold-to-citrate ratio [51]. The synthesized NPs were nearly spherical, (13.2 ± 1.6) nm in diameter, as determined by TEM. The colloidal concentration was estimated to be 1.58 nM (see Supporting Information).

The benefits of using water as solvent in organic and material synthesis have been highlighted [52]. In addition, water-soluble NPs are desirable for biological applications [53]. Therefore, the NPs were functionalized in aqueous media using dendritic disulfides **3** or **4** (Fig. 2a), or the nondendritic disulfide **1** (Fig. 2b); giving rise to NPs modified with different surface derivatization denoted as **NPs-3**, **NPs-4**, and **NPs-1**, respectively. Disulfides **1** and **3** are insoluble in water, whereas disulfide **4** presents limited water solubility. Thus, the modification of NPs was performed in 10% methanol in water and the disulfides were added as methanolic solutions. It has already been shown that the disulfide moiety, *via* self-assembly onto the gold surface, is able to replace the physically adsorbed citrate [51]. The modified NPs then undergo a fast aggregation process, which will be discussed in the following sections.

4.4. Study of the aggregation process undergone by the modified NPs

4.4.1. General trends on optical properties of NP and NP aggregates

The position and intensity of the absorption bands of NPs are strongly influenced by particle geometry, size, particle material, surrounding medium, and also by their interactions with other NPs upon aggregation [54,55]. The localized surface plasmon resonance (LSPR) band of gold NPs in aqueous media is noticed around 520 nm. However, if the colloidal particles aggregate and the distance between aggregating NPs becomes small compared with their radii, a red shifting and broadening of the LSPR band are induced and, depending on the strength of the plasmon coupling, additional resonance bands will appear at wavelengths longer than those of the individual particles [56,57].

Theoretical calculations [58] and experimental observations [56] reveal that effects such as particle size, interparticle distance, and physical parameters like solvent, temperature, and light polarization direction exert a profound influence on the extinction spectra. Indeed, the color change resulting from NP aggregation has shown innumerable applications [3]. Thus, UV–vis spectroscopy is a convenient technique to evaluate the NP aggregation process by following the changes of a suitable LSPR band.

4.4.2. NP dendronization using ***3*** (***NPs-3***)

The aggregation process was initially studied by means of UV–vis spectroscopy, following the change in the NP optical properties

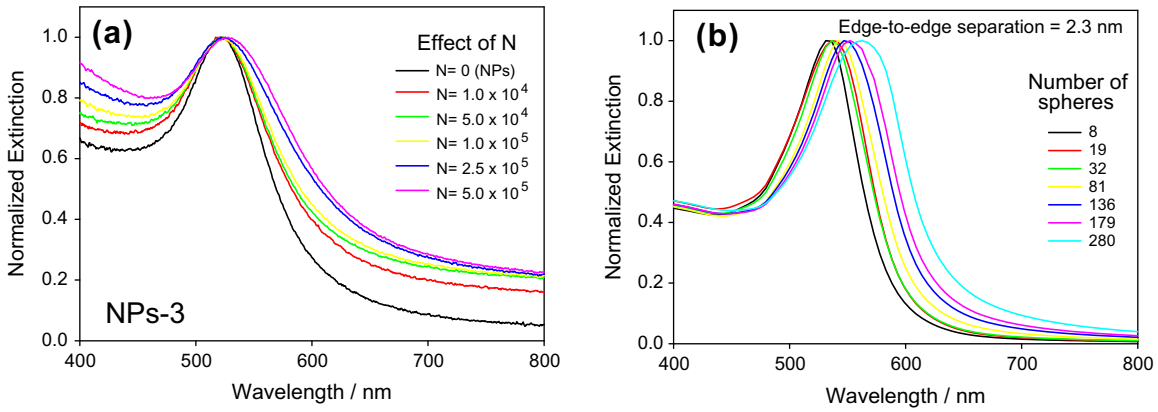

Fig. 3. (a) Spectral change for **NPs-3** as a function of *N*. Conditions: 25 °C, t = 60 min and (b) optical response calculated for sphere clusters with an edge-to-edge separation d = 2.3 nm.

after dendronization using **3** at different concentrations (Fig. 3a). Different values of *N* ranging from $N = 0$ (the unmodified NPs, for reference) to $N = 1 \times 10^6$ were used. For the sake of simplicity, only the spectra taken from $N = 1 \times 10^4$ are shown, since all the spectra for lower *N* are undistinguishable from that of the unmodified NPs.

The formation of **NPs-3** at $N = 1 \times 10^4$ is evidenced by a long tail at higher wavelengths and a slight red shifting, from 521 to 524 nm, of the extinction spectra. A further addition of molecules ($N > 1 \times 10^4$) also induces a red shifting to 529 nm and broadening of the LSPR band. This feature indicates NP aggregation [56]. Interestingly, the extinction spectra for $N < 1 \times 10^4$ (not shown) depicted no significant change on the shape or position of the LSPR peak; this indicates that at those disulfide concentrations, the degree of functionalization of the NP surface is particularly low. Therefore, the average dielectric environment experienced for the modified NPs does not vary and corresponds to the refractive index of the solvent. This result could be explained considering the relative large molecular length and volume of the adsorbed thiolate **3'**, as revealed by our calculations (see Fig. S3).

Even though the surface functionalization degree was low, the dendronized NPs evidenced a noticeable color change: from pink at lower *N* to purplish–violet at higher *N* values. An interesting property of these NP aggregates is their high stability, as they did not precipitate and remained suspended in water for several months. Only when large concentrations of **3** were used in the dendronization ($N \geqslant 1 \times 10^6$), the system did become unstable and the precipitation of large NP aggregates was immediately observed.

Although UV–vis analysis is a useful tool to provide evidence of the aggregation/assembly state of the materials in solution, it is especially difficult to determine using only this technique the aggregate size or structural/size changes produced during the aggregation process [59]. Thus, in order to corroborate that NP aggregation is taking place, DLS and TEM measurements together with theoretical modeling of optical changes induced by aggregation were also performed. Unfortunately, attempts to characterize the obtained materials by other spectroscopic techniques such as IR or NMR were unsuccessful, given the low organic content in the samples.

Therefore, TEM images of stabilized samples of dendronized NPs using different values of *N* were recorded. These micrographs (Fig. 4, left panel) clearly show the formation of larger aggregates as *N* increases. Further valuable evidence of NP aggregation was obtained by performing *in situ* DLS experiments. As depicted in the series of the DLS histograms (Fig. 4, right panel), the volume-weighted distributions show that the relative size of the NP aggregates increases with *N*, in good agreement with UV–vis and TEM results. At $N < 1 \times 10^5$ (Fig. 4a and b), the distribution is governed by free NPs but there are also some aggregates formed. At $N > 1 \times 10^5$ (Fig. 4c–e), the distribution consists mostly of NP aggregates, being the population of isolated NPs almost negligible. Furthermore, DLS results provide a clear qualitative picture about the evolution of the aggregate size as *N* increases, indicating that large aggregates grow up from small ones until a critical size (which depends on the value of *N*) is reached. Strikingly, the most monodisperse samples were those prepared using the highest *N* values (Fig. 4d and e). In view of the previous results, it seems that NP aggregation is a continuous process that takes place until a critical size distribution is attained.

It is worth mentioning that the optical behavior observed as the size of the NP aggregate increases is in good agreement with previous theoretical approaches by Schatz et al. [58,60]. They reported that an increment in the aggregate size, with no decrease in the interparticle distance, leads to a red shifting and broadening of the LSPR band [58]. In the present work, computational simulations of the optical response of gold sphere clusters were calculated and compared with the UV–vis results. A rigorous electrodynamic approach was adopted for sphere clusters taking into account explicitly the coupling of the plasmon modes using the exact Mie solution for the interaction of *n* spheres. In this case, the extinction spectra were calculated for aggregate sizes containing 8–280 gold spheres (13 nm in diameter), arranged in a cubic lattice of a globular shape.

The organic monolayer thickness of the dendronized NP was estimated in 1.15 nm using the calculated molecular length of **3'**. Then, the interparticle distance (d = edge-to-edge separation) in the aggregate was approximated to be twice the molecular length of **3'**, that is, d = 2.3 nm (see Computational Details). The simulated extinction spectra (Fig. 3b) show an excellent qualitative agreement with the UV–vis results (Fig. 3a). As the size of the aggregate increases, a red shifting and broadening of the LSPR band are observed, together with the appearance of a long tail.

Thus, UV–vis, TEM, and DLS studies, together with theoretical simulations conclusively evidence that the process of aggregation of **NPs-3** depends on the value of *N*, being favored with *N* increase.

4.4.3. NP dendronization using ***4*** (***NPs-4***)

In order to favor the aggregation process and to induce a much stronger plasmon coupling among the NPs, the dendronization of NPs with disulfide **4** was performed. This molecule presents terminal carboxylic acid groups instead of the voluminous *t*-Bu ester units of disulfide **3**. This change is expected to significantly enhance NP aggregation due to the possibility of forming hydrogen bonding networks and to the smaller length of the disulfide molecule. This last feature should allow the formation of NP aggregates

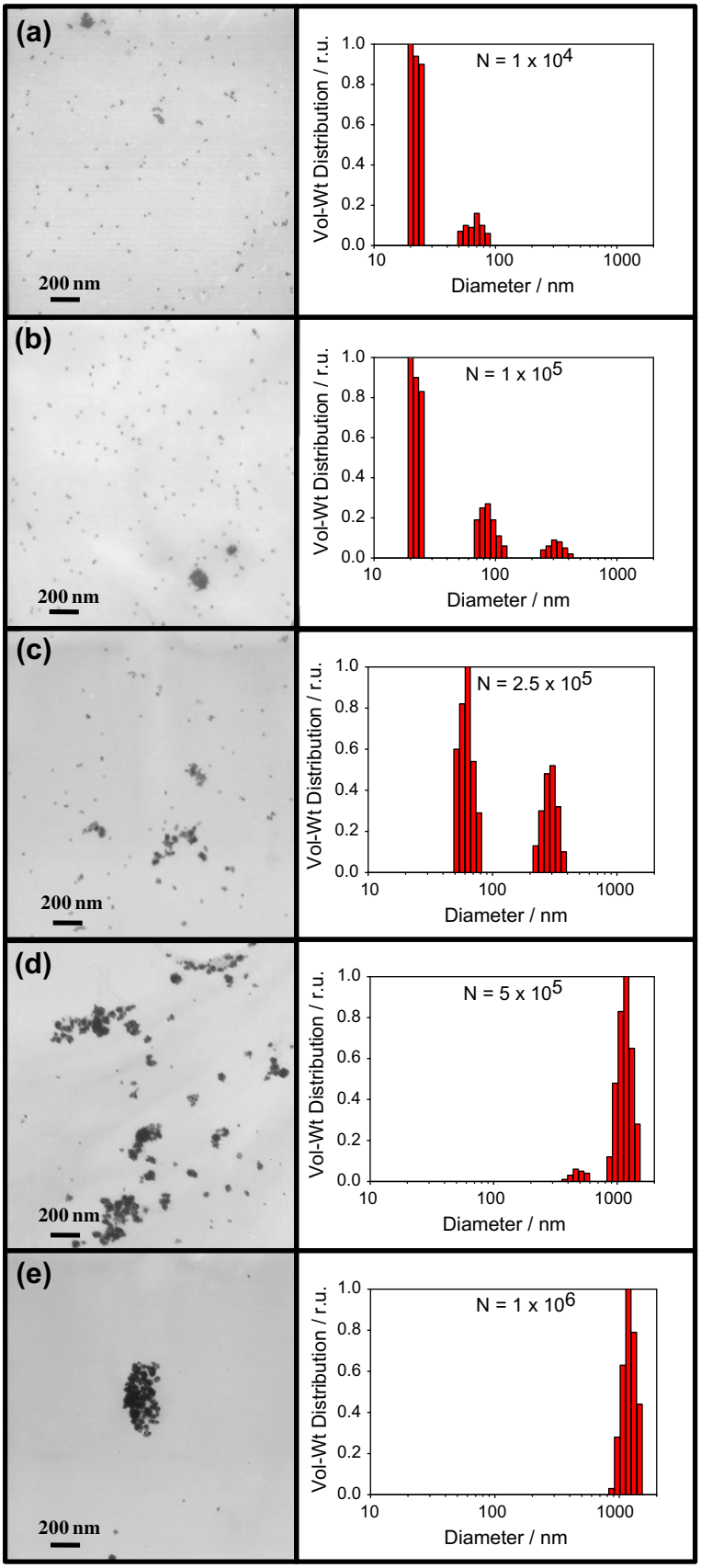

Fig. 4. TEM (left panel) and DLS (right panel) characterization of **NPs-3**. Conditions: 25 °C, *N* values = (a) 1×10^4, (b) 1×10^5, (c) 2.5×10^5, (d) 5×10^5, and (e) 1×10^6. Scale bar = 200 nm.

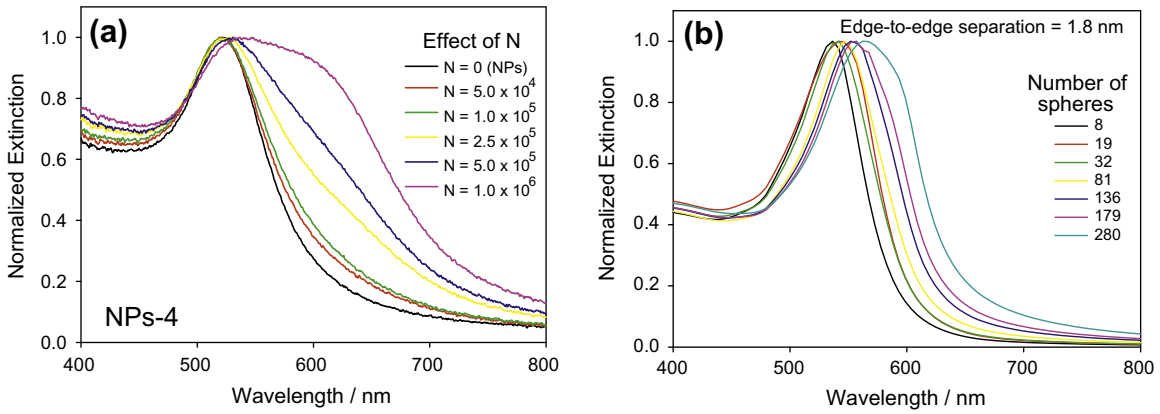

Fig. 5. (a) Spectral change for **NPs-4** as a function of *N*. Conditions: 25 °C, *t* = 60 min and (b) optical response calculated for sphere clusters with an edge-to-edge separation of *d* = 1.8 nm.

with shorter interparticle distances giving rise, as mentioned above, to a stronger plasmonic coupling.

Hence, after NP dendronization using **4,** an appreciable color change was observed, from pink at lower *N* to bluish-violet at the highest *N* values. Moreover, **NPs-4** did not precipitated within the experiments and were stable for several months.

The change in the UV–vis spectra as the NPs were dendronized with **4** was evaluated as a function of *N* (Fig. 5a). In comparison with **NPs-3**, **NPs-4** evidenced a more significant change in the extinction spectra: a more pronounced broadening and redshift of LSPR band, and even the appearance of a new extinction band around 600 nm at higher *N*. These results suggest, as expected, that in **NPs-4** there is a lower interparticle distance and a stronger plasmonic coupling among NPs [3,56]. This can be explained considering that the molecular length of the adsorbed specie **4**′ is lower than the corresponding value of the specie **3**′.

The extinction spectra of sphere clusters were simulated using an interparticle distance *d* = 1.8 nm. The results (Fig. 5b) indicate that, for the same cluster size, a decrease in the interparticle separation produces a greater redshift and broadening of the LSPR, in agreement with the experimental observations. However, the degree of broadening and redshift evidenced by the UV–vis experimental results (Fig. 5a) is by far larger than that predicted by the theoretical calculations (Fig. 5b). Computational restrictions preclude us to perform calculations for clusters of larger size but a higher broadening and redshift should be expected [60], in agreement with the experimental extinction spectra shown in Fig. 5a. Reducing the interparticle distance or averaging the spectra over the size distribution of the NP aggregates should produce the same effect [60]. Although the present calculations did not give quantitative agreement with experiments, they do give a qualitative picture of the main factors controlling the shape and position of the LSRP band. It is expected that due to the nature of the functional groups of disulfide **4**, interactions could be favored not only between terminal groups, but also between terminal and internal moieties. Consequently, a smaller interparticle distance could also be possible, explaining the pronounced change in the UV–vis spectra.

*4.4.4. NP modification with **1** (**NPs-1**)*

NP derivatization using compound **1** was performed only for comparison. This disulfide exhibits an average molecular length of 1.1 nm, is nondendritic (without ramifications), and is expected to form closely and regularly packed structures onto the NP surface [57].

Fig. 6a depicts the noticeable effect that the modification of NPs using **1** produces on their extinction spectra. At $N < 2.5 \times 10^6$, the spectra show a very small LSPR broadening. This remarkable characteristic indicates that the closely and regularly packed monolayer around an individual NP only causes a minor change in the dielectric environment as the size of the organic shell is very small (*ca.* 0.54 nm for the adsorbed specie **1**′) compared to NP diameter (13 nm). Interestingly, at $N > 2.5 \times 10^6$, a dramatic LSPR splitting and broadening in the extinction spectra is observed. This is a sign of the formation of NP aggregates with a relative small interparticle separation and therefore a significant plasmon coupling.

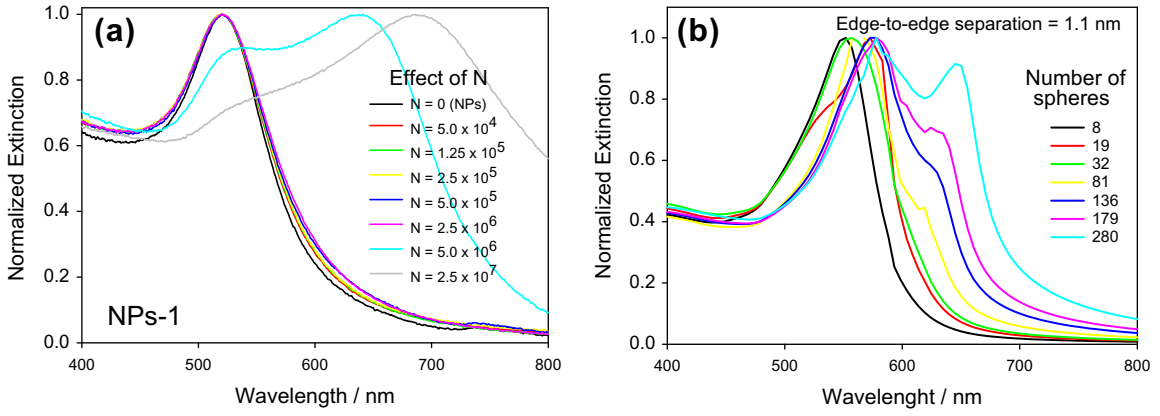

Fig. 6. (a) Spectral change for **NPs-1** as a function of *N*. Conditions: 25 °C, *t* = 60 min and (b) optical response calculated for sphere clusters with an edge-to-edge separation of *d* = 1.1 nm.

Unlike the dendronized-NP aggregates (**NPs-3** and **NPs-4**), which are stable in water solution, the aggregates **NPs-1** are unstable. Indeed, at $N > 5 \times 10^6$, they start to precipitate during the measurements, an effect observed by a drop down in the intensity of the extinction spectra (not shown).

The optical response for the clusters was simulated considering an interparticle separation $d = 1.1$ nm (Fig. 6b). A good qualitative correspondence between the simulated extinction and the measured UV–vis spectra at different N values was found, that is, as the size of the aggregate increases, a redshift, a broadening, and a splitting of the LSPR band are observed, together with the presence of a long tail. In this case, the appearance of a new extinction band around 650 nm was observed at higher N.

4.4.5. Temporal evolution and temperature effects on the NP aggregation

It has been demonstrated in previous sections that after a critical value of N is reached, NP aggregation is induced. Therefore, in the present section, we will attempt to study the kinetics of this process following the variation in the extinction spectra after the addition of a given value of N. The spectra were acquired at 10-min intervals over a period of up to 40–60 min, at a fixed N. Such N value corresponds to the highest N used for each system in order to avoid precipitation: $N = 5 \times 10^5$ for **NPs-3**; $N = 1 \times 10^6$ for **NPs-4**; and $N = 5 \times 10^6$ for **NPs-1**. The temporal evolution of the extinction spectra is shown in Fig. 7.

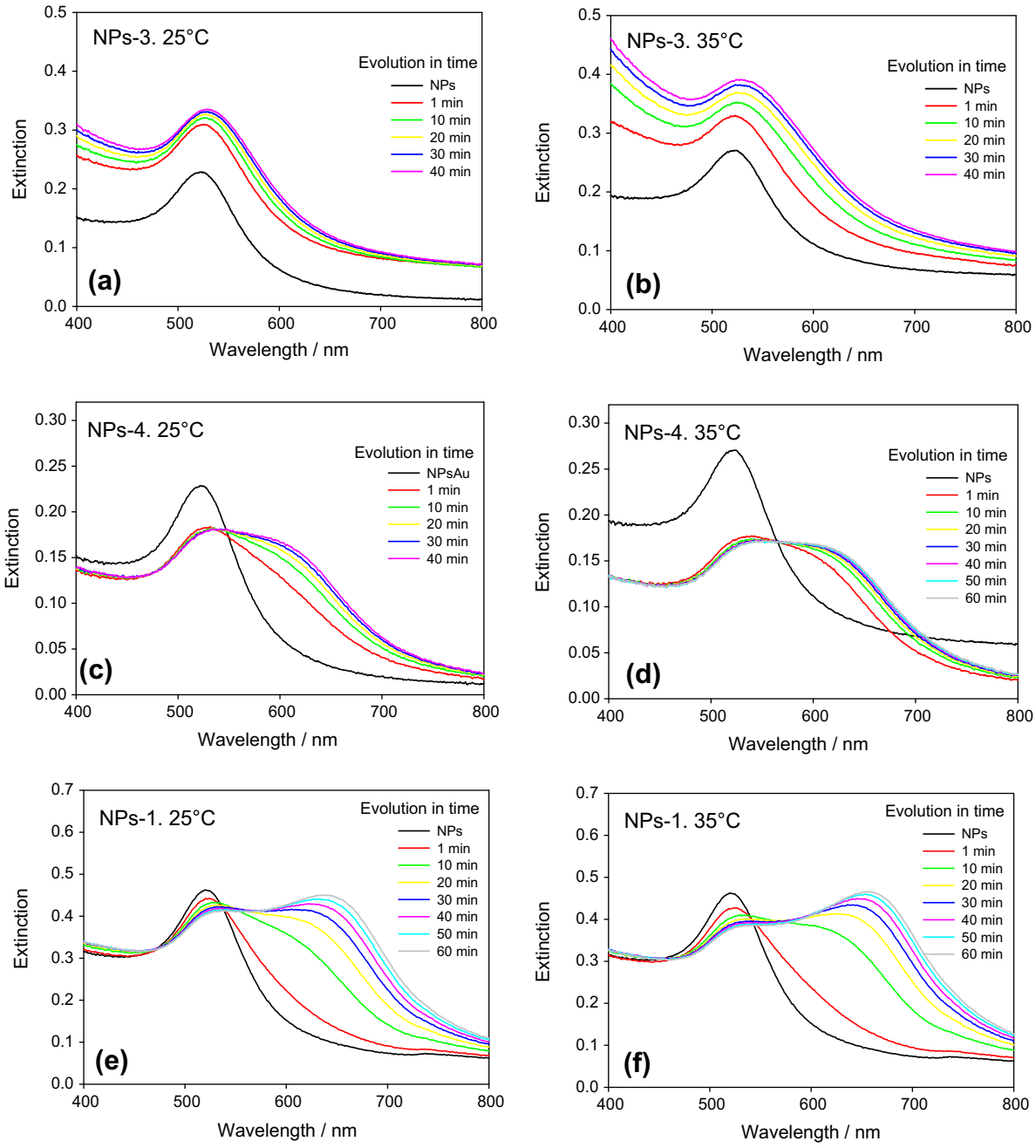

Fig. 7. Time-resolved UV–vis spectra of modified NPs. (a–b) **NPs-3**, (c–d) **NPs-4**, (e–f) **NPs-1**. Conditions: (a–b) $N = 5 \times 10^5$, (c–d) 1×10^6, (e–f) 5×10^6; temperature = 25 °C (a, c, e) and 35 °C (b, d, f).

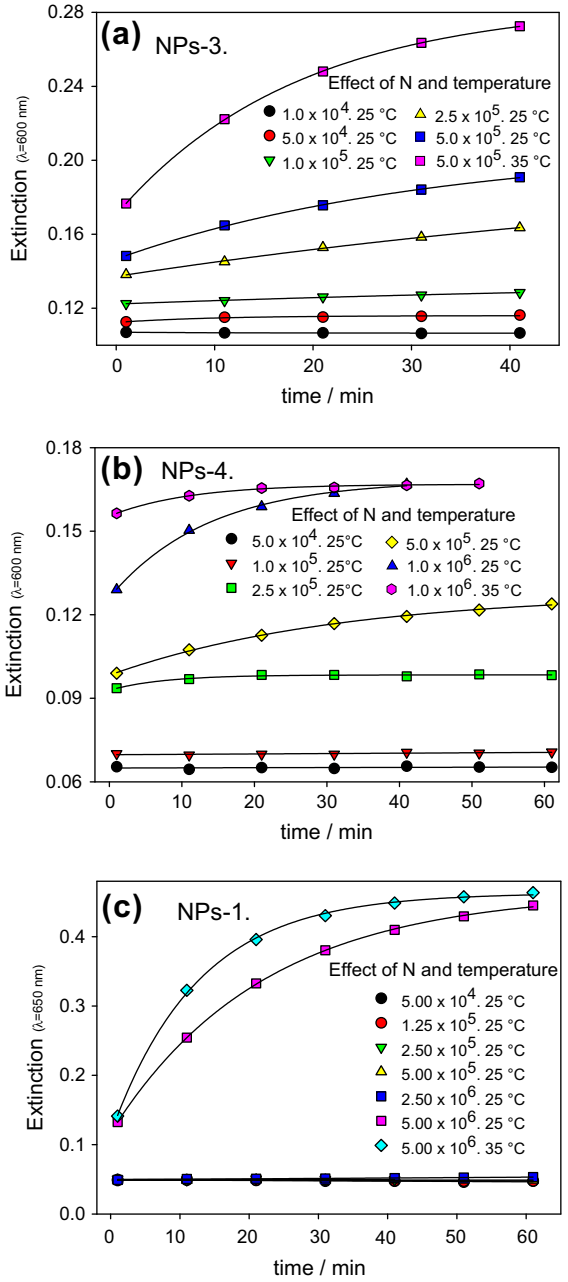

Fig. 8. Kinetics of the NP aggregation process undergone by (a) **NPs-3**, (b) **NPs-4**, and (c) **NPs-1**. The temporal evolution of the extinction peaks was measured at λ = 600 nm, 600 nm and 650 nm, respectively.

It is evident that, regardless the disulfide employed to functionalize the NPs, the NP aggregation process can be temporally followed by noting the spectral broadening and red shifting of the LSPR band, in accordance with other studies. [59,61,62] The degree of spectral change is higher for NP aggregates with the smaller interparticle distance and for NP aggregates with the same interparticle distance, larger at the highest temperature.

Then, to further study the aggregation kinetics, the temporal evolution of the extinction peak intensities at a fixed wavelength was measured (Fig. 8). The determinations were done at different N values, at λ = 600 nm for **NPs-3** and **NPs-4**, and at λ = 650 nm for **NPs-1**. These wavelengths were chosen for each system in such a way that the maximum variation in the extinction is observed.

Fig. 8 shows that the aggregation rate depends on N. At low N, the aggregation of **NPs-3**, **NPs-4**, and **NPs-1** depicts qualitatively the same behavior: the aggregation rate is almost constant. At intermediate N, the aggregation rate increases for **NPs-3** and **NPs-4** but remains constant for **NPs-1**, whereas at high N, it increases for all systems. In addition, the degree of aggregation, taken as the change in the extinction intensity at a fixed evolution time (for example, at t = 20 min) depends on N but also on the nature of the disulfide used as ligand. When dendritic molecules **3** and **4** are used, the degree of aggregation depends on N in all the studied range. When molecule **1** is used, no evidence of NP aggregation until $N \leqslant 2.5 \times 10^6$ is observed; however, at $N = 5.0 \times 10^6$, a very fast aggregation process is induced. This behavior demonstrates that in **NPs-3** and **NPs-4**, the degree of aggregation can be easily controlled by varying N, whereas exerting such a control for **NPs-1** is particularly difficult since a minor change in N triggers an uncontrolled aggregation.

Table 1
Apparent pseudo first-order rate constants calculated for the different NPs aggregates.

NP aggregates	N and temperature conditions		k_{app} ($\times 10^{-2}$ min^{-1})
NPs-3	$N = 2.5 \times 10^5$	25 °C	(1.2 ± 0.4)
	$N = 5.0 \times 10^5$	25 °C	(3.1 ± 0.2)
		35 °C	(5.43 ± 0.07)
NPs-4	$N = 5.0 \times 10^5$	25 °C	(3.2 ± 0.2)
	$N = 1.0 \times 10^6$	25 °C	(7.4 ± 0.7)
		35 °C	(9.2 ± 1.1)
NPs-1	$N = 5.0 \times 10^6$	25 °C	(4.57 ± 0.08)
		35 °C	(8.0 ± 0.2)

The plots shown in Fig. 8 were adjusted to an exponential equation $E = E_0 + Ae^{(-kt)}$, where k represents the apparent pseudo first-order rate constants k_{app} of the aggregation process. Some representative values of k_{app} are listed in Table 1, making possible to quantitatively analyze the dependence of the aggregation kinetics with N and temperature. For a particular aggregate, keeping constant N, k_{app} increases with temperature. Also, from the comparison of the k_{app} calculated for different systems, a few interesting observations can be pointed out. First, if one compares systems having the same number but different kind of terminal functional groups, like **NPs-3** and **NPs-4** under equal dendronization conditions ($N = 5 \times 10^5$, 25 °C), an almost identical k_{app} is observed. Second, if systems having the same kind but different number of functional groups are compared, such as **NPs-4** and **NPs-1**, it is clear that molecule **4** induces a faster aggregation kinetics than molecule **1**. Both disulfides **4** and **1** present the same kind of terminal -COOH moieties but have functionality 3–1. In this context, k_{app} calculated at 25 °C for **NPs-4** at $N = 1 \times 10^6$ and for **NPs-1** at $N = 5.0 \times 10^6$ were compared. Although in these conditions, **NPs-4** contain 40% less of —COOH groups than **NPs-1**, the former presents a k_{app} 1.6 times higher. This difference clearly shows that the aggregation rate of these events depends not only on the number of functional groups but also on the nature of the disulfide used. These results evidence the characteristic multivalent effect of dendritic molecules, which has been previously described, for example, in catalysis [63] or in biological processes like carbohydrate-mediated binding events [64].

5. General discussion

The results show that a good control of the interparticle spacing and the optical properties of NP aggregates can be attained in aqueous media using a dendronization strategy. Our approach takes advantage and joins the benefits of two building blocks, that is, precisely defined dendritic disulfides and size and shape controlled gold NPs. This goal was achieved, first, by synthesizing novel dendritic disulfides with suitable functional groups; second,

by dendronizing NPs using these disulfides, and finally, by analyzing carefully the aggregation process undergone by the dendronized NPs. It allowed us to determine the dendronization parameters that are relevant to control the interparticle spacing and the optical properties of NP aggregates.

Our results indicate that the aggregation process is regulated by four determining factors: (i) nature and (ii) concentration of the disulfide in relation to the concentration of the colloidal dispersion, (iii) time, and (iv) temperature. The nature of the disulfide includes size and molecular architecture (dendritic vs nondendritic) and also functionality, that is, the number and type of terminal functional groups (hydrophilic vs hydrophobic).

The importance of the nature of the capping molecules on the surface of NPs in relation to their directed self-assembly has been recently reviewed, where the occurrence of self-assembly events mediated by hydrophobic forces and hydrogen bonding was shown [1]. In this respect, Nath and Chilkoti [65] reported the functionalization of NPs with mercaptoundecanoic acid onto which an elastin-like polypeptide was adsorbed. The last underwent a thermally triggered hydrophilic-to-hydrophobic phase transition resulting in the formation of large aggregates due to interparticle hydrophobic interaction [65]. On the basis of these results, it might be possible that in aqueous media **NPs-3** undergo an aggregation process based on interparticle hydrophobic interactions. Moreover, several reports can be found on NPs aggregation mediated by hydrogen bonds [6,66,67]. In view of this, it is proposed that the aggregation process followed by **NPs-4** and **NPs-1** might be mediated by hydrogen bonding.

It was shown that the optical properties of NP aggregates are controlled mainly by two effects. Firstly, by the molecular size of the disulfide used as ligand for NP modification. A higher broadening, red shifting, and splitting of the LSPR band are in good agreement with a stronger plasmon coupling, a lower interparticle distance and a smaller ligand. Secondly, the ligand concentration directly controls the assembly process, as was similarly reported by Sethi and Knecht [59].

As it was assumed that the interparticle distance within the aggregates is determined by the geometry of the disulfide bound to the NP surface, the molecular length of the corresponding isolated thiolates was theoretically calculated. These values were used as a reference for the theoretical simulation of the optical response of the sphere clusters, and such results were then compared to the experimental results. The simulated responses were found to correlate well with the experimental UV–vis spectra. An especially good correlation was observed for **NPs-3** (red shifting and broadening of the LSPR band) and **NPs-1** (splitting of the LSPR band). However, for **NPs-4,** such correlation was not as good as previously found. In this particular case, the theoretical optical response calculated for an interparticle distance of 1.8 nm only indicates the characteristic red shifting and broadening of the LSPR band, whereas the experimental results also show the splitting of such band. This difference suggests that the interparticle distance in **NPs-4** is probably lower than that estimated in 1.8 nm, used as reference on the basis of the molecular size calculated for the corresponding thiolate **4′**. A possible explanation for this result might be the interdigitation of the dendritic chains of **4′** within the aggregate in which the terminal —COOH moieties of one dendritic molecule can interact by hydrogen bonds, not only with the —COOH end groups but also with the amide groups located in the inner part of a neighboring molecule.

In addition, the temporal evolution of all NP aggregates was analyzed observing their growth by means of UV–vis. Furthermore, the TEM and DLS studies performed over stabilized aggregated samples of **NPs-3** suggest that the larger aggregates are likely to grow at the expense of the smaller ones, since the presence of isolated NPs or smaller aggregates was almost negligible for highly aggregated samples (high *N*). These results are in good agreement with other studies in the literature [59]. It was also found that an increase in temperature causes faster aggregation in all cases, as evidenced by UV–vis experiments. This is consistent with the aggregation process of a cross-linking system in which kinetics is dominated by random collisions between NPs with a relatively slow Brownian motion [68].

A further important characteristic found in the present work is the variation in the stability of the aggregates and the control that could be exerted over the assembly process by changing the nature of the ligand molecule: a more effective control was attained when dendritic disulfides were employed, which suggests that the molecular architecture plays a significant role in the assembly process. The dendronization of NPs, using ligands **3** and **4**, allows controlling the degree of aggregation by varying the disulfide concentration in a very wide range and gives rise to colloidal dispersions, which are stable in solution for several months. The size of the aggregate in this case could be particularly large as demonstrated by our DLS and TEM characterizations. Conversely, the functionalization of NPs using the nondendritic disulfide **1** produces much less controlled NP aggregates and leads to unstable dispersions that precipitate in a few minutes. In order to analyze this difference in the stability of the NP aggregates, it is necessary to consider two aspects: (1) the structure/geometry adopted by dendritic molecules in solution and (2) the characteristics presented by the organic monolayer formed on the NPs after the functionalization process was carried out.

Previous studies have shown that low-generation dendritic molecules adopt an open structure, while high-generation ones have a more globular geometry in solution [69]. This effect was elegantly demonstrated in a work by Pietsch et al. [70] where oligosaccharide-modified dendrimers were used to template NP synthesis. The authors showed that the size (generation) and structure (open vs globular) of the dendritic molecule directly control the formation and the mechanism of stabilization of the NPs. Besides, Zhang et al. [57] recently studied how the organic monolayer formed onto NPs is affected by the ramification of the ligand used. They found that the use of branched ligands for NP functionalization leads to the formation of organic layers with lower packing density than that obtained from the analog molecules without ramifications [57]. Moreover, this effect has been explained for the case of NPs initially stabilized with citrate ions as in the present work. As demonstrated, the degree of displacement of citrate ions is lower for ligands exhibiting a lower packing density; the remaining citrate ions fill void spaces on the NP surface and thus lead to enhanced NP stabilization in water/THF solution [57]. Wang et al. [23] also associated the high photochemical stability of dendronized NPs with the ramification of the ligands used and Piao et al. [71] reported that the conformational freedom presented by the ligands or surfactants employed plays an important role in the dispersion stability of NPs. In fact, the dispersion stability of NPs stabilized with *n*-alkyl chain monodentate surfactants is generally poor, since they tend to pack densely, and hence lose the conformational entropy of the surfactant layer. Therefore, the introduction of disorder into the protecting organic monolayer has shown to increase the steric hindrance and to enhance the dispersion stability of NPs [71,72]. In this context, the use of multidentate alkanethiols [57] or kinked ligands like oleic acid [73] has proved to be useful.

We attribute the high stability of the NP aggregates **NPs-3** and **NPs-4** to the open, multibranched and flexible geometry characteristic of the dendritic ligands **3** and **4** employed in the present work. The use of dendritic ligands leads to the formation of NPs stabilized with a disordered organic layer with lower packing density and to a low degree of replacement of citrate ions; the remaining citrate ions fill void spaces on the NP surface. All these factors contribute

to enhance the stability of the formed NP aggregates. Otherwise, the use of high concentrations of the unbranched smaller-size ligand **1** leads to the formation of an ordered organic layer with a higher packing density, to a significant degree of replacement of citrate ions, and consequently to the formation of very unstable NP aggregates in water. These results clearly demonstrate that the dendronization of NPs is a valid and powerful strategy that permits the preparation of stable multifunctional NP aggregates.

Finally, it should be remarked that the intrinsic multifunctional nature of the dendritic molecules allows having a high number of functional groups decorating the NP surface using a low concentration of ligands. This characteristic is closely related to the stability mentioned above and offers the possibility of controlling the NP aggregate size by varying the ligand concentration.

6. Conclusions

Is this work, the usefulness of applying the dendronization of NPs to generate controlled NP aggregates has been demonstrated. In order to achieve this goal, two dendritic disulfides were synthesized and used to prepare stable NP aggregates with controlled size and optical properties in aqueous media. The key role played by different dendronization parameters like the ligand nature and concentration, temperature, and time over the size and stability control of the formed NP aggregates was demonstrated. In particular, the stability of the resulting NP aggregates showed to be dependent on the nature of the disulfide used (dendritic vs non-dendritic). The higher stability of the aggregates prepared from dendronized NPs was explained on the basis on the open, flexible and disordered structure that dendritic molecules present in the organic layer located at the NP surface. Besides, comparative experiments carried out using a linear disulfide analog led to the formation of uncontrolled and unstable NP aggregates.

The stable multifunctional NP aggregates prepared in this work with certain control over their size could be promising candidates for several applications including optical devices, optical (bio)sensors, colorimetric assays, and enhanced spectroscopies.

Acknowledgments

The authors would like to thank Dr. Gloria Bonetto for technical assistance with NMR experiments, Dr. Diego Andrada for computational calculations of molecular structures, and Dr. Verónica Brunetti for proofreading the article. Financial support from CONICET, ANPCyT, and SECYT-UNC is gratefully acknowledged. J.I.P. thanks CONICET for the fellowship provided.

Appendix A. Supplementary material

Supplementary data associated with this article can be found, in the online version, at http://dx.doi.org/10.1016/j.jcis.2012.06.034.

References

[1] M. Grzelczak, J. Vermant, E.M. Furst, L.M. Liz-Marzán, ACS Nano 4 (2010) 3591.
[2] S.I. Lim, C.-J. Zhong, Acc. Chem. Res. 42 (2009) 798.
[3] S.K. Ghosh, T. Pal, Chem. Rev. 107 (2007) 4797.
[4] N.L. Rosi, C.A. Mirkin, Chem. Rev. 105 (2005) 1547.
[5] K. Saha, S.S. Agasti, C. Kim, X. Li, V.M. Rotello, Chem. Rev. Article ASAP (2012).
[6] C.A. Mirkin, R.L. Letsinger, R.C. Mucic, J.J. Storhoff, Nature 382 (1996) 607.
[7] K. Aslan, J.R. Lakowicz, C.D. Geddes, Anal. Chim. Acta 517 (2004) 139.
[8] N. Uehara, K. Ookubo, T. Shimizu, Langmuir 26 (2010) 6818.
[9] Y.-R. Kim, R.K. Mahajan, J.S. Kim, H. Kim, ACS Appl. Mater. Interf. 2 (2010) 292.
[10] Y. Wei, S. Han, J. Kim, S. Soh, B.A. Grzybowski, J. Am. Chem. Soc. 132 (2010) 11018.
[11] M.E. Stewart, C.R. Anderton, L.B. Thompson, J. Maria, S.K. Gray, J.A. Rogers, R.G. Nuzzo, Chem. Rev. 108 (2008) 494.
[12] S.M. Grayson, J.M.J. Fréchet, Chem. Rev. 101 (2001) 3819.
[13] D.K. Smith, A.R. Hirst, C.S. Love, J.G. Hardy, S.V. Brignell, B. Huang, Prog. Polym. Sci. 30 (2005) 220.
[14] A.D. Schlüter, J.P. Rabe, Angew. Chem. Int. Edit. 39 (2000) 864.
[15] M. Martinelli, M. Calderón, C.I. Alvarez I, M.C. Strumia, React. Funct. Polym. 67 (2007) 1018.
[16] M. Martinelli, M. Calderón, E. Rodríguez, J.J. Freire, M.C. Strumia, Eur. Polym. J. 43 (2007) 1978.
[17] J.C. Cuggino, M. Calderón, C.I. Alvarez, M.C. Strumia, K.N. Silva, E.K. Penott-Chang, A.J. Müller, J. Colloid Interf. Sci. 357 (2011) 147.
[18] J.I. Paez, P. Froimowicz, A.M. Baruzzi, M.C. Strumia, V. Brunetti, Electrochem. Commun. 10 (2008) 541.
[19] J.I. Paez, M.C. Strumia, M.C.G. Passeggi Jr., J. Ferrón, A.M. Baruzzi, V. Brunetti, Electrochim. Acta 54 (2009) 4192.
[20] J.I. Paez, A.L. Cappelletti, A.M. Baruzzi, V. Brunetti, M.C. Strumia, Macromol. Symp. 290 (2010) 37.
[21] J.I. Paez, M. Martinelli, V. Brunetti, M.C. Strumia, Polymers 4 (2012) 355.
[22] R. Wang, J. Yang, Z. Zheng, M.D. Carducci, J. Jiao, S. Seraphin, Angew. Chem. Int. Edit. 40 (2001) 549.
[23] Y.A. Wang, J.J. Li, H. Chen, X. Peng, J. Am. Chem. Soc. 124 (2002) 2293.
[24] M.-K. Kim, Y.-M. Jeon, W.S. Jeon, H.-J. Kim, S.G. Hong, C.G. Park, K. Kim, Chem. Commun. (2001) 667.
[25] K.R. Gopidas, J.K. Whitesell, M.A. Fox, J. Am. Chem. Soc. 125 (2003) 6491.
[26] M.-C. Daniel, J. Ruiz, S. Nlate, J.-C. Blais, D. Astruc, J. Am. Chem. Soc. 125 (2003) 2617.
[27] D. Choi, L. Chinn, Y.S. Shon, Polym. Mater. Sci. Eng. 93 (2005) 739.
[28] G. Jiang, L. Wang, T. Chen, H. Yu, C. Chen, Mater. Chem. Phys. 98 (2006) 76.
[29] C.S. Love, V. Chechik, D.K. Smith, C. Brennan, J. Mater. Chem. 14 (2004) 919.
[30] G. Palui, S. Ray, A. Banerjee, J. Mater. Chem. 19 (2009) 3457.
[31] V.K. Ratheesh Kumar, K.R. Gopidas, Chem-Asian J. 5 (2010) 887.
[32] F. González De Rivera, L.I. Rodríguez, O. Rossell, M. Seco, N.J. Divins, I. Casanova, J. Llorca, J. Organomet. Chem. 696 (2011) 2287.
[33] T. Joon Cho, R.A. Zangmeister, R.I. MacCuspie, A.K. Patri, V.A. Hackley, Chem. Mater. 23 (2011) 2665.
[34] L.M. Bronstein, Z.B. Shifrina, Chem. Rev. 111 (2011) 5301.
[35] C.S. Love, I. Ashworth, C. Brennan, V. Chechik, D.K. Smith, J. Colloid Interf. Sci. 302 (2006) 178.
[36] H. Yan, C. Wong, A.R. Chianese, J. Luo, L. Wang, J. Yin, C.-J. Zhong, Chem. Mater. 22 (2010) 5918.
[37] H. Xu, S. Srivastava, V.M. Rotello, Adv. Polym. Sci. 207 (2007) 179.
[38] B.L. Frankamp, A.K. Boal, V.M. Rotello, J. Am. Chem. Soc. 124 (2002) 15146.
[39] S. Srivastava, B.L. Frankamp, V.M. Rotello, Chem. Mater. 17 (2005) 487.
[40] B. Pan, F. Gao, L. Ao, H. Tian, R. He, D. Cui, Colloids Surf., A 259 (2005) 89.
[41] J. Turkevich, P.C. Stevenson, J. Hillier, Discuss. Faraday Soc. 11 (1951) 55.
[42] M.J. Frisch, G.W. Trucks, H.B. Schlegel, G.E. Scuseria, M.A. Robb, J.R. Cheeseman, J.A.J. Montgomery, T. Vreven, K.N. Kudin, J.C. Burant, J.M. Millam, S.S. Iyengar, J. Tomasi, V. Barone, B. Mennucci, M. Cossi, G. Scalmani, N. Rega, G.A. Petersson, H. Nakatsuji, M. Hada, M. Ehara, K. Toyota, R. Fukuda, J. Hasegawa, M. Ishida, T. Nakajima, Y. Honda, O. Kitao, H. Nakai, M. Klene, X. Li, J.E. Knox, H.P. Hratchian, J.B. Cross, C. Adamo, J. Jaramillo, R. Gomperts, R.E. Stratmann, O. Yazyev, A.J. Austin, R. Cammi, C. Pomelli, J.W. Ochterski, P.Y. Ayala, K. Morokuma, G.A. Voth, P. Salvador, J.J. Dannenberg, V.G. Zakrzewski, S. Dapprich, A.D. Daniels, M.C. Strain, O. Farkas, D.K. Malick, A.D. Rabuck, K. Raghavachari, J.B. Foresman, J.V. Ortiz, Q. Cui, A.G. Baboul, S. Clifford, J. Cioslowski, B.B. Stefanov, G. Liu, A. Liashenko, P. Piskorz, I. Komaromi, R.L. Martin, D.J. Fox, T. Keith, M.A. Al-Laham, C.Y. Peng, A. Nanayakkara, M. Challacombe, P.M.W. Gill, B. Johnson, W. Chen, M.W. Wong, C. Gonzalez, J.A. Pople, Revision C.02 ed. ed.; Gaussian, Inc., Wallingford CT, 2004.
[43] M.J.S. Dewar, W. Thiel, J. Am. Chem. Soc. 99 (1977) 4907.
[44] C. Peng, P.Y. Ayala, H.B. Schlegel, M.J. Frisch, J. Comput. Chem. 17 (1996) 49.
[45] This is only an approximation in order to work with a more simplified model. However, it should be noted that it has been previously reported the occurrence of sulfur atoms bound to one and two gold atoms (see Ref. [46]).
[46] P.D. Jadzinsky, G. Calero, C.J. Ackerson, D.A. Bushnell, R.D. Kornberg, Science 318 (2007) 430.
[47] H. Grönbeck, J. Phys. Chem. C 114 (2010) 15973.
[48] Y.L. Xu, Appl. Opt. 36 (1997) 9496.
[49] E.R. Encina, E.A. Coronado, J. Phys. Chem. C 114 (2010) 3918.
[50] C.S. Love, I. Ashworth, C. Brennan, V. Chechik, D.K. Smith, Langmuir 23 (2007) 5787.
[51] S.Y. Lin, Y.T. Tsai, C.C. Chen, C.M. Lin, C.H. Chen, J. Phys. Chem. B 108 (2004) 2134.
[52] C.-J. Li, in: Green Chemical Syntheses and Processes, American Chemical Society, 2000, p. 62.
[53] J.C. Love, L.A. Estroff, J.K. Kriebel, R.G. Nuzzo, G.M. Whitesides, Chem. Rev. 105 (2005) 1103.
[54] L.M. Liz-Marzán, Mater. Today 7 (2004) 26.
[55] K.L. Kelly, E. Coronado, L.L. Zhao, G.C. Schatz, J. Phys. Chem. B 107 (2003) 668.
[56] A.N. Shipway, M. Lahav, R. Gabai, I. Willner, Langmuir 16 (2000) 8789.
[57] S. Zhang, G. Leem, L.O. Srisombat, T.R. Lee, J. Am. Chem. Soc. 130 (2008) 113.
[58] A.A. Lazarides, G.C. Schatz, J. Phys. Chem. B 104 (2000) 460.
[59] M. Sethi, M.R. Knecht, ACS Appl. Mater. Int. 1 (2009) 1270.
[60] J.J. Storhoff, A.A. Lazarides, R.C. Mucic, C.A. Mirkin, R.L. Letsinger, G.C. Schatz, J. Am. Chem. Soc. 122 (2000) 4640.
[61] Y. Yang, S. Matsubara, M. Nogami, J. Shi, Mater. Sci. Eng. B – Adv. 140 (2007) 172.
[62] C. Guarise, L. Pasquato, P. Scrimin, Langmuir 21 (2005) 5537.

[63] E. Delort, T. Darbre, J.-L. Reymond, J. Am. Chem. Soc. 126 (2004) 15642.
[64] E. Arce, P.M. Nieto, V. Díaz, R. García Castro, A. Bernad, J. Rojo, Bioconjugate Chem. 14 (2003) 817.
[65] N. Nath, A. Chilkoti, J. Am. Chem. Soc. 123 (2001) 8197.
[66] C.H. Bernard Ng, J. Yang, W.Y. Fan, J. Phys. Chem. C 112 (2008) 4141.
[67] Z. Peng, T. Walther, K. Kleinermanns, Langmuir 21 (2005) 4249.
[68] K. Sato, K. Hosokawa, M. Maeda, J. Am. Chem. Soc. 125 (2003) 8102.
[69] G. Caminati, N.J. Turro, D.A. Tomalia, J. Am. Chem. Soc. 112 (1990) 8515.
[70] T. Pietsch, D. Appelhans, N. Gindy, B. Voit, A. Fahmi, Colloids Surf., A 341 (2009) 93.
[71] L. Piao, K.H. Lee, W.J. Kwon, S.H. Kim, S. Yoon, J. Colloid Interf. Sci. 334 (2009) 208.
[72] R. Balasubramanian, B. Kim, S.L. Tripp, X. Wang, M. Lieberman, A. Wei, Langmuir 18 (2002) 3676.
[73] K.S. Suslick, M. Fang, T. Hyeon, J. Am. Chem. Soc. 118 (1996) 11960.